

A SHELL/3D MODELING TECHNIQUE FOR DELAMINATIONS IN COMPOSITE LAMINATES

Ronald Krueger

National Research Council Research Associate

NASA Langley Research Center

Hampton, VA 23681

ABSTRACT

A shell/3D modeling technique was developed for which a local solid finite element model is used only in the immediate vicinity of the delamination front. The goal was to combine the accuracy of the full three-dimensional solution with the computational efficiency of a plate or shell finite element model. Multi-point constraints provide a kinematically compatible interface between the local 3D model and the global structural model which has been meshed with plate or shell finite elements. For simple double cantilever beam (DCB), end notched flexure (ENF), and single leg bending (SLB) specimens, mixed mode energy release rate distributions were computed across the width from nonlinear finite element analyses using the virtual crack closure technique. The analyses served to test the accuracy of the shell/3D technique for the pure mode I case (DCB), mode II case (ENF) and a mixed mode I/II case (SLB). Specimens with a unidirectional layup where the delamination is located between two 0° plies, as well as a multidirectional layup where the delamination is located between two non-zero degree plies, were simulated. For a local 3D model extending to a minimum of about three specimen thicknesses in front of and behind the delamination front, the results were in good agreement with mixed mode strain energy release rates obtained from computations where the entire specimen had been modeled with solid elements. For large built-up composite structures modeled with plate elements, the shell/3D modeling technique offers a great potential, since only a relatively small section in the vicinity of the delamination front needs to be modeled with solid elements.

INTRODUCTION

One of the most common failure modes for composite structures is delamination. The remote loadings applied to composite components are typically resolved into interlaminar tension and shear stresses at discontinuities that create mixed-mode I and II delaminations. Over the past two decades, the onset and growth of these delaminations has been characterized using fracture mechanics [1-2]. The total strain energy release rate, G , the mode I component due to interlaminar tension, G_I , and the mode II component due to interlaminar shear, G_{II} , are calculated from continuum (2D)

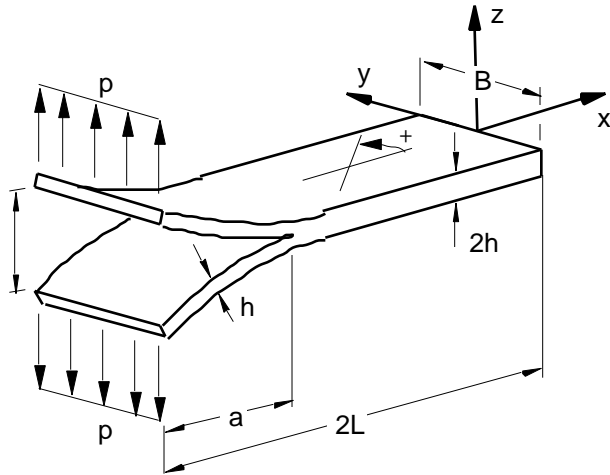
and solid (3D) finite element analyses using the virtual crack closure technique [3-5]. In order to predict delamination onset or growth, these calculated G components are compared to interlaminar fracture toughness properties measured over a range from pure mode I loading to pure mode II loading. Since many layers of brick elements through the thickness are often necessary to model the individual plies, the size of finite element models required for accurate analyses may become prohibitively large. To improve computational efficiency, built-up structures are therefore traditionally modeled and analyzed using plate or shell finite elements. Computed mixed mode energy release rate components, however, depend on many variables, such as element order and shear deformation assumptions, kinematic constraints in the neighborhood of the delamination front, and continuity of material properties and section stiffness in the vicinity of the debond when delaminations or debonds are modeled with plate or shell finite elements [4,6]. For example, in reference 6, mesh refinement studies showed that computed G_I , G_{II} , and G_{III} did not converge when the structure above and below the plane of delamination was modeled with plate elements with different section properties (thickness or layup). These problems may be avoided by using three dimensional models. Furthermore, three dimensional analyses are required when matrix cracks and multiple delaminations need to be modeled at different ply interfaces. Therefore, methods based on 3D modeling to calculate fracture parameters in built-up structures need to be improved.

The objective of the current work is to develop a shell/3D modeling technique for which a local solid finite element model is used only in the immediate vicinity of the delamination front and the remainder of the structure is modeled using plate or shell elements. The goal of the shell/3D technique is to combine the computational efficiency of a plate or shell finite element model with the accuracy of the full three-dimensional solution in the areas of interest. Multi-point constraints provide a kinematically compatible interface between the local 3D model and the surrounding global structural model, which can be meshed with plate or shell finite elements. The shell/3D technique proposed is validated for the pure mode I case, mode II case and a mixed mode I/II case using the double cantilever beam (DCB), end notched flexure (ENF), and single leg bending (SLB) specimens respectively (see Figure 1). For each specimen, mixed mode energy release rate distributions were computed across the width from nonlinear finite element analyses using the virtual crack closure technique [3-5]. The results were compared with mixed mode strain energy release rates obtained from computations where the entire specimen had been modeled with solid elements.

ANALYSIS FORMULATION

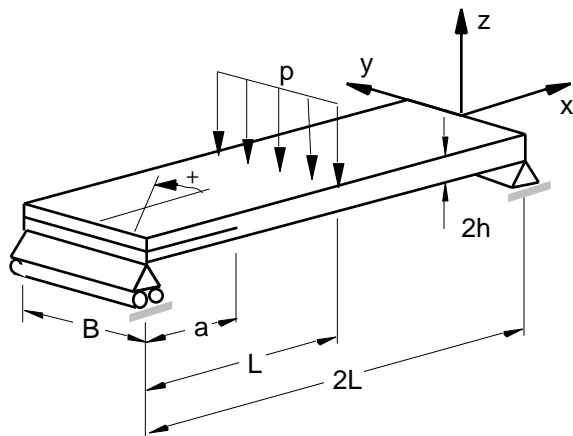
Finite Element Analysis

The goal of this investigation was to study the accuracy of the shell/3D modeling technique by comparing energy release rates computed using the shell/3D modeling technique to results obtained from full three-dimensional models. A shell/3D model of a DCB specimen is shown in Figure 2. For the entire investigation, the ABAQUS® geometric nonlinear analysis procedure was used. The global section was modeled with ABAQUS® four-noded quadrilateral shell elements, type S4. The local 3D section and the full three-dimensional model were modeled with ABAQUS® solid eight-noded incompatible mode elements, type C3D8I, to prevent shear locking. A combination of reduced integrated eight-noded quadrilateral shell elements S8R with solid twenty-noded hexahedral elements C3D20R was also studied. The transition from the global shell element model to the local three-dimensional model in the vicinity of the delamination front was accomplished by using multi-point constraints to enforce appropriate translations and rotations at the shell-solid interface [7].



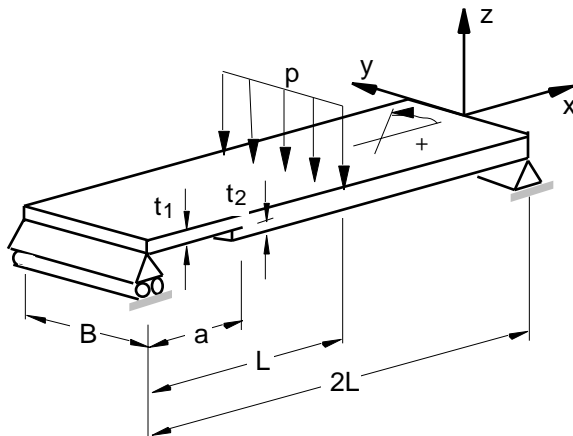
	UD24	D±30
B	25.0 mm	25.4 mm
2h	3.0 mm	4.06 mm
2L	150.0 mm	150.0 mm
a	111.5 mm	57.2 mm
P	12.66 N	10.0 N

(a) Double Cantilever Beam Specimen (DCB)



	D±30
B	25.5 mm
2h	4.06 mm
2L	127.0 mm
a	31.8 mm
P	100.0 N

(b) End Notched Flexure Specimen (ENF)



	UD32
B	25.0 mm
t ₁	2.03 mm
t ₂	2.03 mm
2L	177.8 mm
a	34.3 mm
P	100.0 N

(c) Single Leg Bending Specimen (SLB)

FIGURE 1. Specimen Configurations.

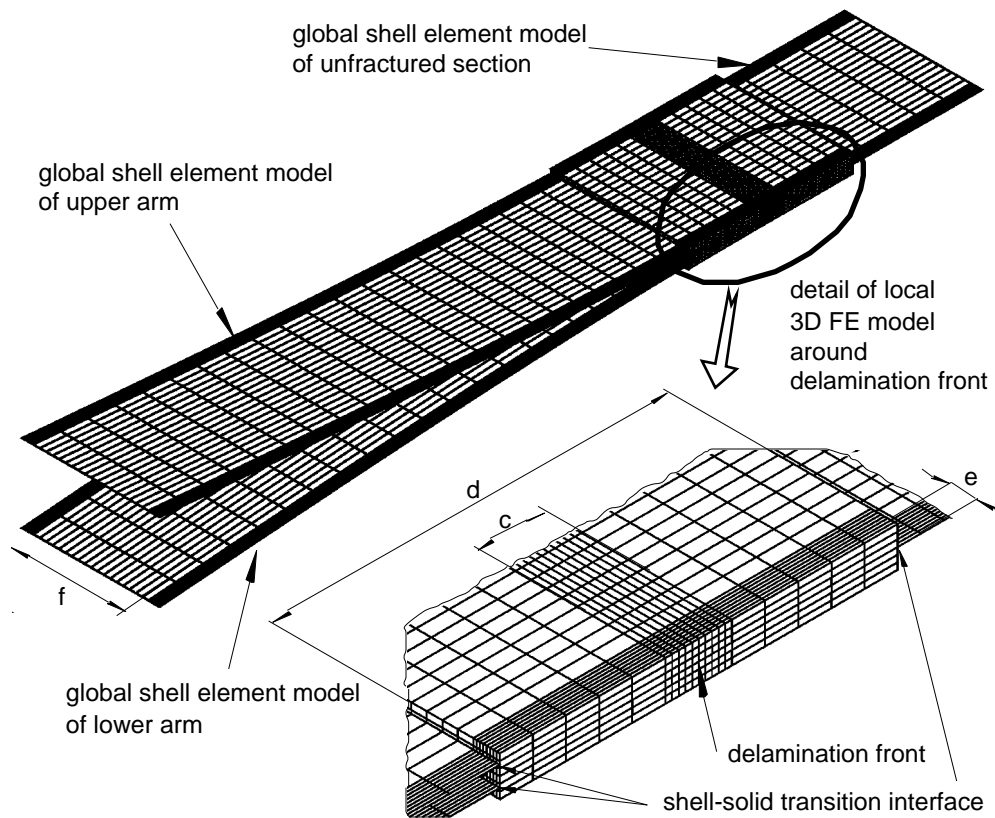


FIGURE 2. Finite Element Model of DCB Specimen

A typical FE model and a detailed view are shown in Figure 2. Three lay ups were studied. They were designated UD32, with layup $[0]_{32}$, $D\pm 30$, with a multidirectional layup $[\pm 30/0/-30/0/30/0_4/30/0/-30/0/-30/30/-30/30/0/30/0/-30/0_4/30/0/30/0/\pm 30]$ and UD24, with layup $[0]_{24}$. The arrow denotes the location of the delamination, which for all three lay ups was located in the midplane. The UD32 and $D\pm 30$ layup were made of C12K/R6376 graphite/epoxy and the UD24 layup was made of T300/1076 graphite/epoxy. The material properties are given in Table 1. The specimens with unidirectional layup were modeled by six elements through the specimen thickness. For the specimens with $D\pm 30$ layup, two plies on each side of the delamination were modeled individually using one element for each ply. The adjacent four plies were modeled by one element with material properties smeared using the rule of mixtures. The adjacent element extended over the four 0° plies. The six outermost plies were modeled by one element with smeared material properties. The delamination was modeled as a discrete discontinuity in the center of the specimen, with separate, unconnected nodes (with identical coordinates) on the upper and lower surfaces of the delaminated section. Referring to figure 2, the specimen with UD24 layup was divided into a center section of width $f=21.0$ mm with 18 elements ($D\pm 30$: $f=21.4$ mm, 10 elements, UD32: $f=24.2$ mm, 20 elements) and two refined edge sections $e=2.0$ mm with 8 elements ($D\pm 30$: $e=2.0$ mm, 8 elements, UD32: $e=0.4$ mm, 5 elements) to capture local edge effects and steep gradients. These sections appear as dark areas in the full view of the specimen as shown in Figure 2. Along the length a refined mesh of length $c=5$ mm with 10 elements ($D\pm 30$: $c=3.0$ mm, 12 elements, UD32: $c=6.0$ mm, 24 elements) was used in the vicinity of the delamination front. This section length, c , was kept constant during the entire investigation. To study the

TABLE 1. MATERIAL PROPERTIES

T300/1076 Unidirectional Graphite/Epoxy Prepreg [8]		
$E_{11} = 139.4$ GPa	$E_{22} = 10.16$ GPa	$E_{33} = 10.16$ GPa
$\nu_{12} = 0.30$	$\nu_{13} = 0.30$	$\nu_{23} = 0.436$
$G_{12} = 4.6$ GPa	$G_{13} = 4.6$ GPa	$G_{23} = 3.54$ GPa
C12K/R6376 Unidirectional Graphite/Epoxy Prepreg [8]		
$E_{11} = 146.9$ GPa	$E_{22} = 10.16$ GPa	$E_{33} = 10.16$ GPa
$\nu_{12} = 0.33$	$\nu_{13} = 0.33$	$\nu_{23} = 0.33$
$G_{12} = 5.45$ GPa	$G_{13} = 5.45$ GPa	$G_{23} = 3.99$ GPa

influence of the size of the local zone on computed mixed mode energy release rates, the total size of the local zone modeled with solid elements, d , was varied ($d=10, 15, 20, 25, 30$ mm). For the simulation of the ENF and SLB specimens, interpenetration of the delamination faces was prevented by using contact elements [7].

Virtual Crack Closure Technique

The Virtual Crack Closure Technique (VCCT) was used to calculate strain energy release rates for the delaminations [3-5]. The mode I, mode II and mode III components of the strain energy release rate, G_I , G_{II} and G_{III} , were calculated for eight noded solid elements as shown in Figure 3

$$G_I = -\frac{1}{2} \frac{1}{A} Z_{Li} (w_{L\ell} - w_{L\ell}') \quad (1)$$

$$G_{II} = -\frac{1}{2} \frac{1}{A} X_{Li} (u_{L\ell} - u_{L\ell}') \quad (2)$$

$$G_{III} = -\frac{1}{2} \frac{1}{A} Y_{Li} (v_{L\ell} - v_{L\ell}') \quad (3)$$

with $A = ab$ [5]. Here A is the area virtually closed, a is the length of the elements at the delamination front and b is the width of the elements. The X'_{Li} , Y'_{Li} and Z'_{Li} denote the forces at the delamination front in column L , row i , and $u'_{K\ell}$, $v'_{K\ell}$ and $w'_{K\ell}$ are the relative displacements at the corresponding node row ℓ behind the delamination front as shown in Figure 3. For geometrically nonlinear analysis, both forces and displacements were transformed into a local coordinate system (x' , y'), that defined the normal and tangential coordinate directions at the delamination front in the deformed configuration. Additional information with respect to the application of the VCCT and equations for twenty noded solids are given in the literature [3-6].

Care must be exercised in interpreting the values for G_I , G_{II} and G_{III} obtained using the virtual crack closure technique for interfacial delaminations between two orthotropic solids [9]. For the delamination in the $+30^\circ/-30^\circ$ ply interface, the element length a was chosen to be about twice the ply thickness, $t=0.127$ mm and this element length was used consistently during the entire investigation.

COMPUTED ENERGY RELEASE RATES

For the mode I DCB specimen with unidirectional layup (UD24), strain energy release rate distributions across the width are shown in Figure 4. As expected, the mode II and mode III strain energy release rates are computed to be nearly zero and hence are not shown. In this figure the G distribution is shown for the combination of twenty noded brick elements in the local 3D model with eight noded shell elements

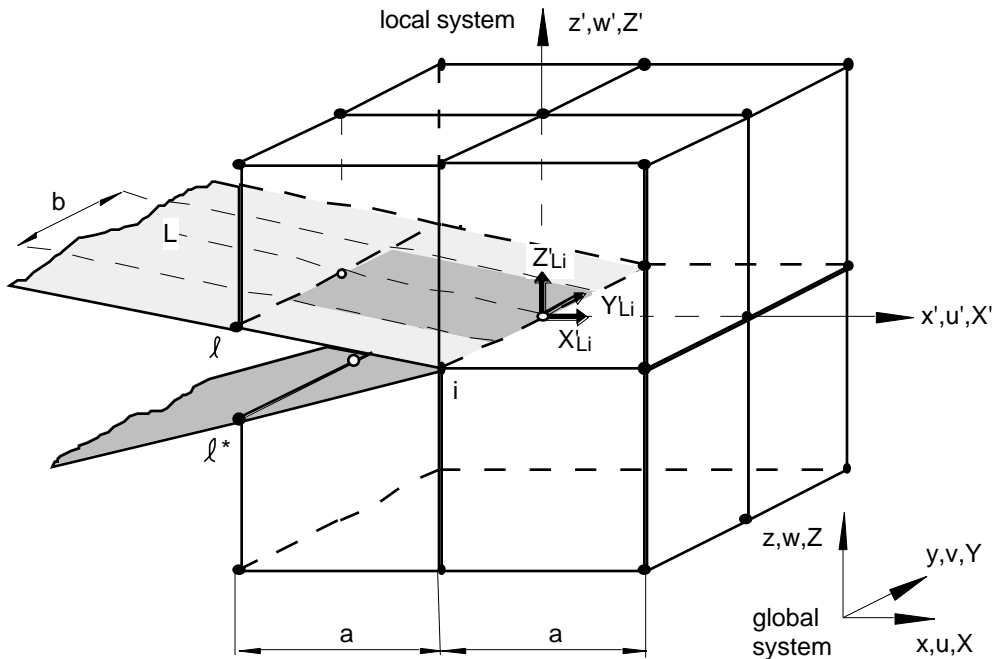


FIGURE 3. Virtual Crack Closure Technique for Eight Noded Elements.

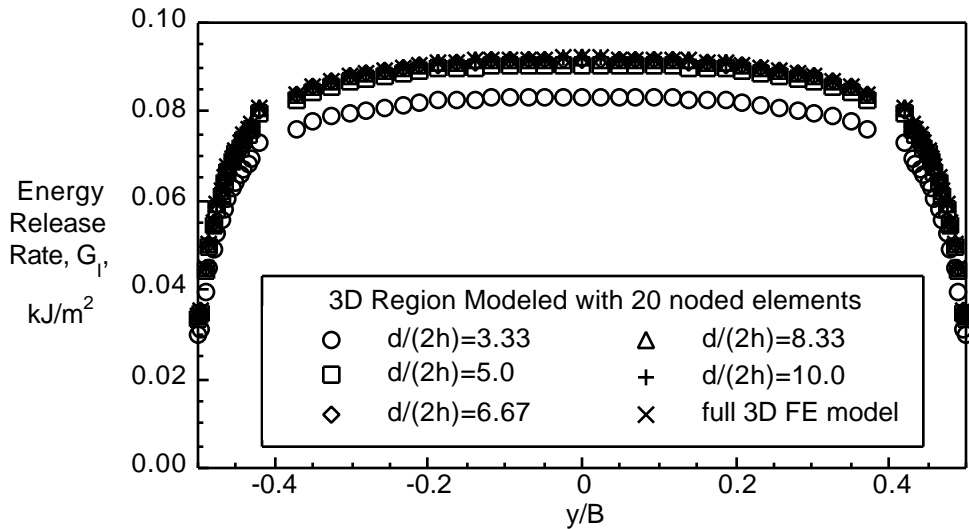


FIGURE 4. Strain Energy Release Rate Distribution Across the Width of a UD24-DCB Specimen Modeled with 20 Noded Elements.

in the global model. With increasing size of the local 3D model, d , computed results from the shell/3D model converge to the solution obtained from a full 3D model. For a local 3D model extending to a minimum of about three specimen thicknesses in front and behind the delamination front ($d/2h=6.67$), the results were within 1% of the mixed mode strain energy release rates obtained from computations where the entire specimen had been modeled with solid elements. The shell/3D model is capable of accurately simulating the anticlastic bending effect that causes the energy release rate to be highest in the center of the specimen and lowest at its edges. Results for the combination of eight noded brick elements with four noded shell elements are shown in Figure 5. When compared to the model with twenty noded solids and eight noded

shell elements, the combination of eight noded brick elements with four noded shell elements yields identical results and provides a reduced model size. For ENF and SLB specimens with unidirectional layup, strain energy release rates were also identical for both combinations of solid and shell elements. Therefore, the combination of eight noded brick elements with four noded shell elements was used for the remainder of this study.

For all specimens with $D\pm 30$ layup, the size of the local model was chosen to be $d=25$ mm. This size corresponds to about three specimen thicknesses in front and behind the delamination front ($d/2h=6.16$). For this length/thickness ratio the solution was within 1% of the 3D results for the DCB-UD24 case discussed earlier. As shown in Figure 6 for the DCB- $D\pm 30$ specimen, the zone with a constant G_I distribution in the center becomes smaller compared to the UD24 case and the drop towards the edges is more pronounced. The drop is caused by increased anticlastic bending due to the lower values of bending rigidities in the individual arms for this layup [10]. Again, as expected, the computed mode II and mode III values are nearly zero and

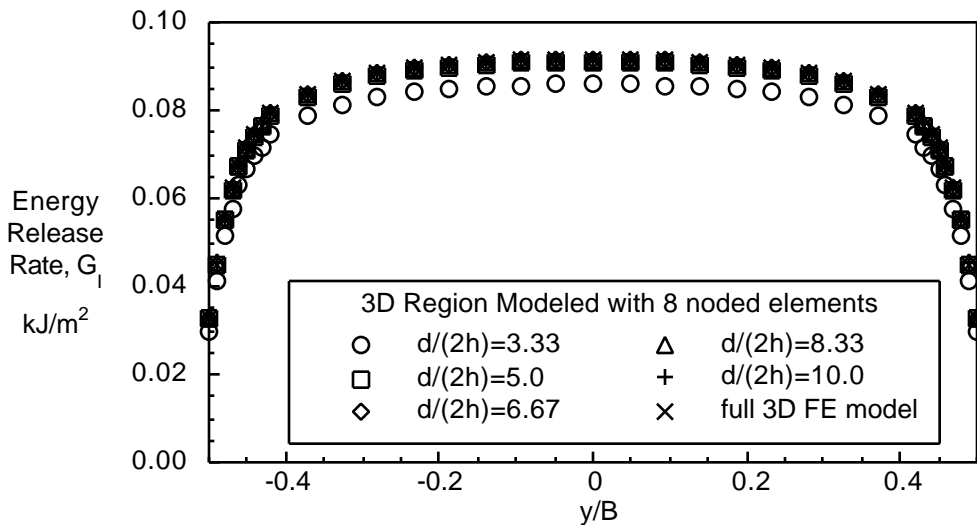


FIGURE 5. Strain Energy Release Rate Distribution Across the Width of a UD24-DCB Specimen Modeled with 8 Noded Elements.

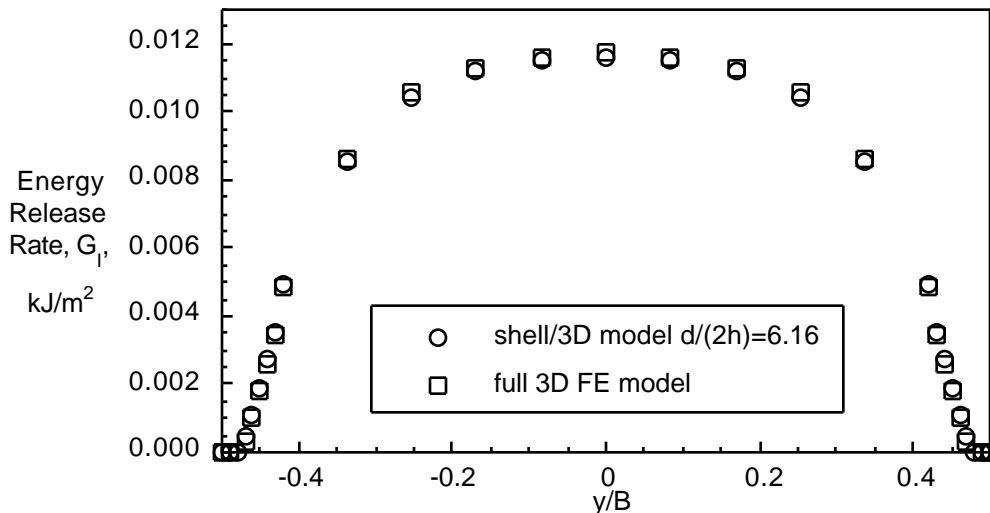


FIGURE 6. Strain Energy Release Rate Distribution Across the Width of a DCB Specimen With $D\pm 30$ Layup.

hence are not shown in the figure. The good agreement with results obtained from full 3D models suggests that these effects are accurately simulated by the shell/3D model.

For the mode II ENF tests, references 8 and 10 show that the mode II energy release rate is fairly constant across almost the entire width of the specimen, peaking in the immediate vicinity of the edges and accompanied by local mode III contributions in the same areas. These peaks become more visible for specimens with multidirectional layup [8,10]. Therefore an ENF specimen with $D_{\pm 30}$ layup was selected for this study to verify the accuracy of the shell/3D technique in simulating this local mixed mode case near the edge of the specimen. The mixed mode strain energy release rates shown in Figure 7 confirm that results obtained from a local 3D model extending about three specimen thicknesses in front and behind the delamination front were in good agreement with results obtained from a full 3D model. The computed G_I values are nearly zero and therefore are not shown.

The single leg bending (SLB) specimen, as shown in Figure 1(c), was studied for the determination of fracture toughness as a function of mixed mode I/II ratio [8,11]. A specimen with UD32 layup was selected for this study to verify that the shell/3D modeling technique is also capable of accurately simulating the mixed mode I/II case. The size of the local model was chosen to be $d=25$ mm, which corresponds to a ratio $d/2h=6.16$. The distribution of the mode I energy release rate calculated for a SLB specimen with UD32 layup, shown in Figure 8, resembles the distribution shown in Figures 4 and 5 for the DCB specimen. The mode I energy release rate is fairly constant in the center of the specimen and drops towards the edges. As shown in Figure 9, the computed mode II contribution is nearly constant across almost the entire width of the specimen, with larger values in the immediate vicinity of the edges, accompanied by small values of mode III in the same areas. As before, the results from the shell/3D technique were within 1% of the reference solution obtained from computations where the entire specimen had been modeled with solid elements.

In the current investigation, the application of the shell/3D technique reduced the number of degrees of freedom by about 35% compared to a full 3D model for all three specimen types. For large built-up composite structures modeled with plate elements, the shell/3D modeling technique offers great potential since only a relatively small section in the vicinity of the delamination front needs to be modeled with solid elements. A significant reduction in model size can be expected compared to a full 3D

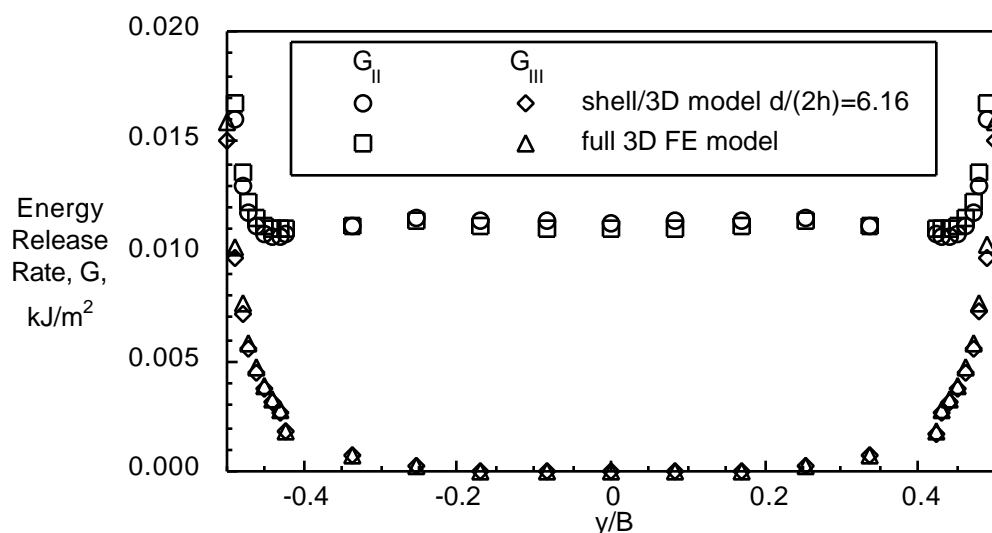


FIGURE 7. Strain Energy Release Rate Distribution Across the Width of an ENF Specimen With $D_{\pm 30}$ Layup.

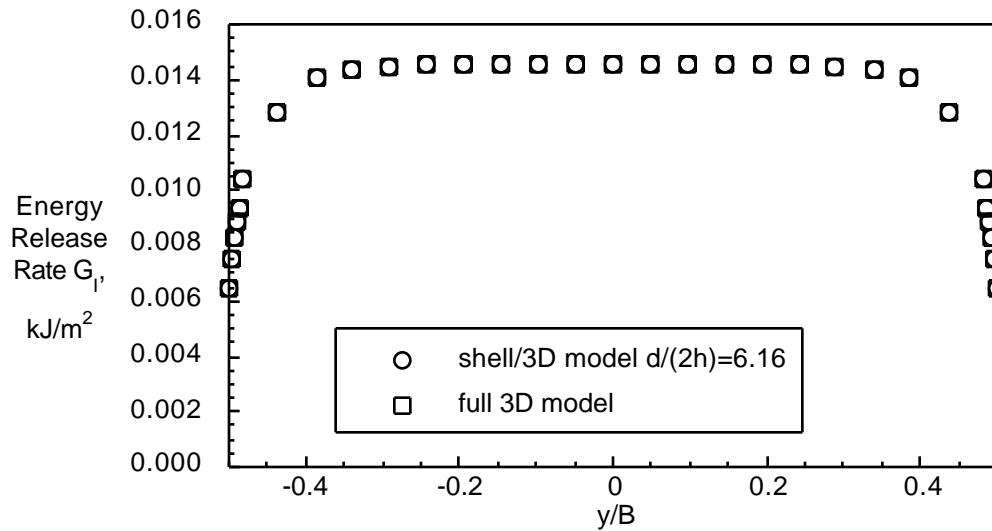


FIGURE 8. Mode I Strain Energy Release Rate Distribution Across the Width of a SLB Specimen Made of UD32 Layup.

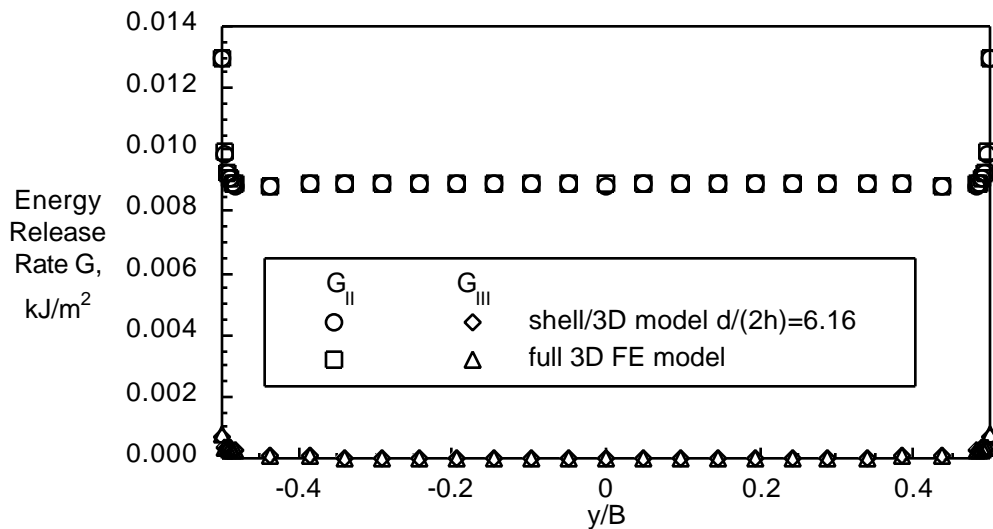


FIGURE 9. Mode II and III Strain Energy Release Rate Distribution Across the Width of a SLB Specimen Made of UD32 Layup.

model. Additionally, already existing plate models may be modified to shell/3D models thus providing the accuracy of a full 3D FE model without requiring the creation of an entirely new three dimensional finite element model.

CONCLUDING REMARKS

A shell/3D modeling technique is presented for the analysis of composite laminates with delaminations. The analysis evaluates the individual mode and total strain energy release rates all along the delamination front. In this analysis a local solid finite element model is used only in the immediate vicinity of the delamination front. The goal was to combine the accuracy of the full three-dimensional solution with the computational efficiency of the plate or shell finite element model. Multi-point constraints provide a kinematically compatible interface between the local 3D model and the global structural model which was meshed with plate or shell finite elements. For the current investigation, two shell/3D combinations were studied: eight noded

solid elements in the local section combined with four noded shell elements in the global section of the model and twenty-noded solid elements in the local section combined with eight-noded shell elements in the global section. The shell elements were connected to the local 3D model using multi-point constraints to enforce appropriate translations and rotations. The geometrically nonlinear solution option of the ABAQUS[®] finite element code was used for the entire investigation.

For simple DCB, ENF, and SLB specimens, mixed mode energy release rate distributions were computed across the width from nonlinear finite element analyses using the virtual crack closure technique. This served to validate the shell/3D modeling technique for the pure mode I case (DCB), mode II case (ENF) and a mixed mode I/II case (SLB). Specimens with a unidirectional layup, for which the delamination is located between two 0° plies, as well as a multidirectional layup for which the delamination is located between two non-zero plies, were simulated. Finite element analyses showed that the accuracy achieved depends on the size of the local area. With increasing size of the local 3D model, the computed results converged towards the energy release rates obtained from full 3D finite element analysis for all specimens, layups and element types simulated. The results were in good agreement with the reference solution once the local zone was extended to about three times the specimen thickness in front and behind the delamination front. For large built-up composite structures modeled with plate elements the shell/3D modeling technique offers great potential since only a relatively small section in the vicinity of the delamination front needs to be modeled with solid elements. Existing plate models may be modified to shell/3D models, which is a considerable advantage compared to the creation of an entirely new three dimensional finite element model.

REFERENCES

- [1] O'Brien, T.K., "Characterization of Delamination Onset and Growth in a Composite Laminate," *Damage in Composite Materials, ASTM STP 775*, 1982, pp. 140-167.
- [2] Martin, R. H., "Incorporating Interlaminar Fracture Mechanics Into Design," International Conference on Designing Cost-Effective Composites, IMechE Conference Transactions, London, 15-16 September, 1998, pp. 83-92.
- [3] Rybicki, E.F. and Kanninen, M.F., "A Finite Element Calculation of Stress Intensity Factors by a Modified Crack Closure Integral", *Eng. Fracture Mech.*, 9, 1977, pp. 931-938.
- [4] Raju, I.S., Sistla, R. and Krishnamurthy, T., "Fracture Mechanics Analysis For Skin-Stiffener Debonding", *Eng. Fracture Mech.*, 54, 1996, pp. 371-385.
- [5] Buchholz, F.G., Grebner, H., Dreyer, K.H. and Krome, H., "2D- and 3D-Applications of the Improved and Generalized Modified Crack Closure Integral Method", *Computational Mechanics '88*, Atluri, S.N. and Yagawa, G., eds., Springer Verlag, 1988,
- [6] Glaessgen, E.H., Riddell, W.T., and Raju, I.S., "Effect of Shear Deformation and Continuity on Delamination Modeling with Plate Elements", *Proceedings of the AIAA/ASME/ASCE/AHS/ASC 39th SSDM Conference*, AIAA-98-2023-CP, 1998.
- [7] ABAQUS/Standard, *User's Manual, Volume II*, Version 5.6, 1996.
- [8] Krüger, R., "Three Dimensional Finite Element Analysis of Multidirectional Composite DCB, SLB and ENF Specimens," ISD-Report No. 94/2, University of Stuttgart, 1994.
- [9] Raju, I. S., Crews, J.H. and Aminpour, M.A., "Convergence of Strain Energy Release Rate Components for Edge-Delaminated Composite Laminates," *Eng. Fracture Mech.*, 30, 1988, pp. 383-396.
- [10] Davidson, B.D., Krüger, R. and König, M., "Three Dimensional Analysis of Center Delaminated Unidirectional and Multidirectional Single Leg Bending Specimens," *Composites Science and Technology*, 1995, 54(4), pp. 385-394.
- [11] Davidson, B.D., Krüger, R. and König, M., "Effect of Stacking Sequence on Energy Release Rate Distributions in Multidirectional DCB and ENF specimens," *Eng. Fracture Mech.*, 1996, 55(4), pp. 557-569.